Assessing the impact of arid area urbanization on flash floods using GIS, remote sensing, and HEC-HMS rainfall–runoff modeling

Mohamed El Alfy

ABSTRACT

This study uses an integrated approach, bringing together geographic information system (GIS), remote sensing, and rainfall–runoff modeling, to assess the urbanization impact on flash floods in arid areas. Runoff modeling was carried out as a function of the catchment characteristics and the maximum daily rainfall parameters. Land-use types were extracted from the supervised classification of SPOT-5 (2010) and Landsat-8 (2015) satellite images and were validated during field checks. Catchment morphometric characteristics were carried out using the correlated Topaz and Arc-Hydro tools. Maximum floods of the catchment were evaluated by coupling GIS and remote sensing with Hydrologic Engineering Center–Hydrologic Modeling System (HEC-HMS) hydrologic modeling. Peak discharges were estimated, and the abstraction losses were computed for different return periods. The model results were calibrated according to actual runoff event. The research shows that rapid urbanization adversely affects hydrological processes, since the sprawl on the alluvial channels is significant. This reduces infiltration into the underlying alluvium and increases runoff, leading to higher flood peaks and volumes even for short duration low intensity rainfall. To retain a considerable amount of water and sediments in these arid areas, construction of small dams at the fingertip channels at the outlet of the lower order sub-basins is recommended.

Key words | flash floods, GIS, rainfall–runoff modeling, remote sensing, urbanization

Mohamed El Alfy
CPSIPW, Prince Sultan Institute for Environmental, Water and Desert Research,
King Saud University,
Riyadh,
Kingdom of Saudi Arabia
and
Geology Department,
Mansoura University,
Mansoura,
Egypt
E-mail: *melalfy@ksu.edu.sa*

INTRODUCTION

Flash flood assessment is a vital issue for establishing properly sustainable development in arid areas. Flash floods are defined as the fast flooding of water, often combined with debris transport, that usually takes place in high gradient streams (Jarrett 1990; Borga *et al.* 2007). Floods result in a variety of hazardous phenomena associated with consequential problems (Cooke *et al.* 1982; El Alfy 1998; Tooth 2000; Chin & Gregory 2001; Oba 2001; Herschy 2002; Foody *et al.* 2004; Ozturk *et al.* 2013). Reliable prediction of runoff in arid areas is difficult to obtain for ungauged basins, since there is a lack of hydro-meteorological data and the gauging of flash floods is very rare (Rodier 1985; Sorman & Abdulrazzaq 1993; Al-Qurashi *et al.* 2008; El Bastawesy *et al.* 2009, 2012; Ozturk *et al.* 2013).

doi: 10.2166/nh.2016.133

Flash flood frequencies and magnitudes are controlled by the interaction of different variables including rainfall, catchment antecedent conditions, and spatial distribution of land-uses. Urbanization in basin areas can be added as an additional significant controlling factor for the development of flash floods. It can increase the risk of flooding due to increased peak discharge and volume, and decreased time to peak (Campana & Tucci 2001; Liu *et al.* 2004; Nirupama & Simonovic 2007; Saghafian *et al.* 2008; Al-Ghamdi *et al.* 2012). Urban watersheds, on an average, lose 90% of storm rainfall to runoff (Shang & Wilson 2009).

In the absence of hydro-meteorological data, runoff modeling could be a promising approach to enhance the livability of an area (Gheith & Sultan 2002; Foody *et al.* 2004). For predicting

hydrologic responses in ungauged catchments, Soil Conservation Service curve number (SCS-CN) models are widely used (SCS 1972). This method had since been adapted to measure infiltration losses in arid areas with similar climatic and physiographic conditions (Reich 1963; Graf 1988; Walters 1990; Al-Khalaf 1997). These SCS models are considered to be as good, or even better than, more complex models in terms of predicting rainfall–runoff in gauged and ungauged catchments (Michaud & Sorooshian 1994; Al-Khalaf 1997; Wagener *et al.* 2004; Dawod *et al.* 2011; Dawod & Koshak 2011; Hublart *et al.* 2015). The Hydrologic Engineering Center–Hydrologic Modeling System (HEC-HMS) is designed to simulate the precipitation–runoff processes of watershed systems (USACE 2010). The input data for this HEC-HMS model setup include digital elevation model (DEM), rainfall, flow gage data, soil types, land-use/land-cover data, etc. The resultant hydrographs are used to study water availability, urban drainage, flow forecasting, future urbanization impact, reservoir spillway design, flood damage reduction, floodplain regulation, and systems operation.

This study uses an integrated approach, bringing together remote sensing, geographic information system (GIS), and hydrological models, which are utilized to assess the impact of urbanization on flash floods in arid areas. The analyses presented in this study are concerned with the estimation of extreme flows, which form the basis for subsequent flood level and mapping stages of the study area. Comparing flood peaks after development to flood peaks before development, over a range of return periods, can be used as a function of

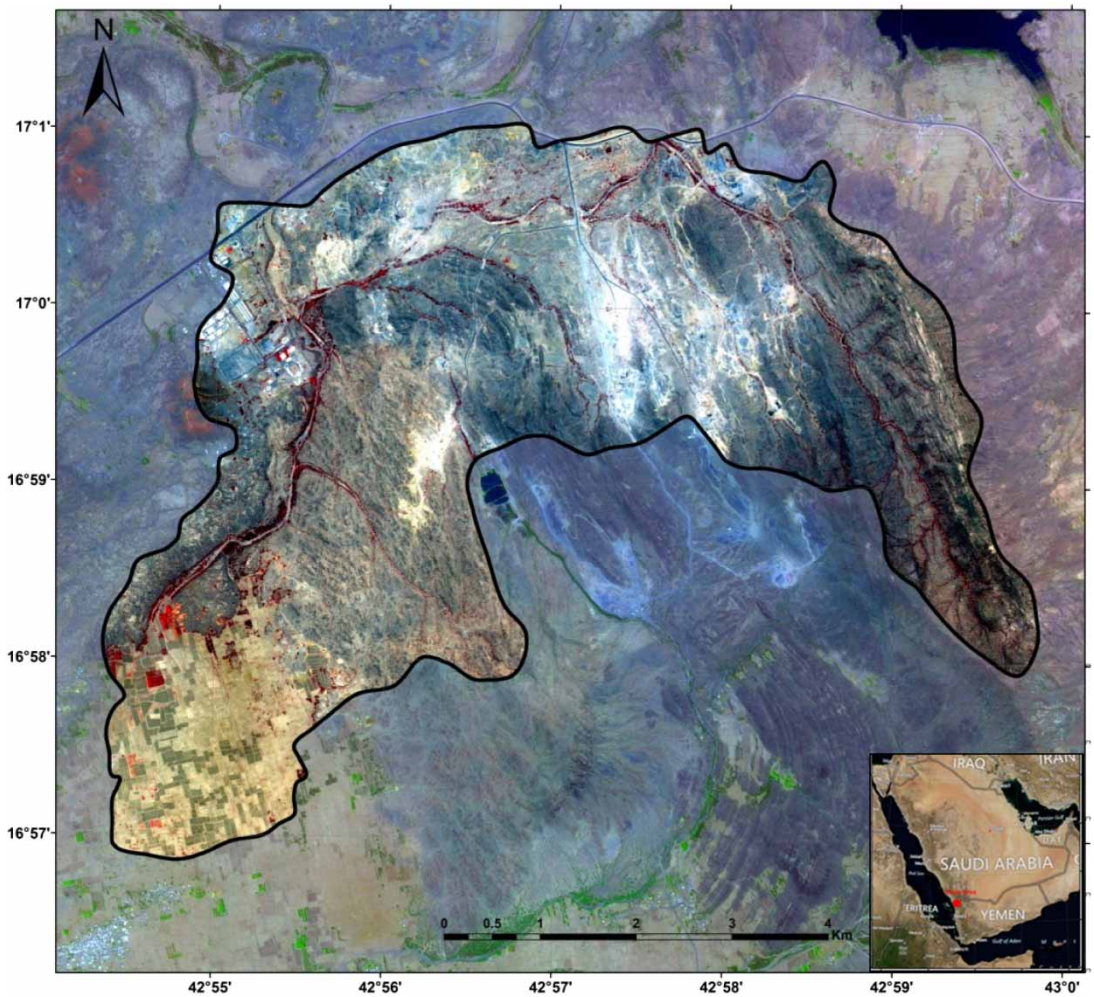

Figure 1 | Location map of the study area, multi-spectral SPOT-5 image (2.5 m pixels).

urbanization impact (Kibler *et al.* 2007). This study will aid in the decision-making for future planning and the results of this work can help to prioritize areas where flood control measures should be directed, and effectively augment management plans for the appropriate development of water resources.

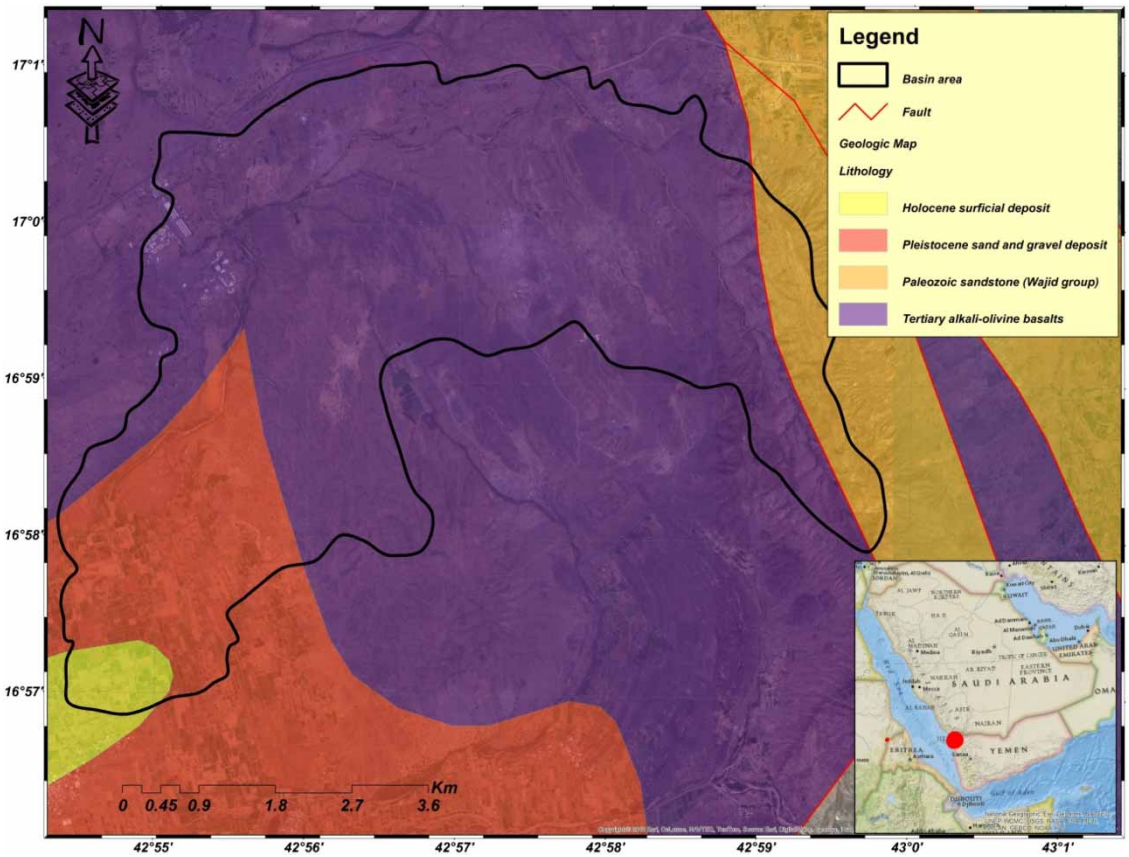

Figure 2 | Geologic map of the study area (Blank & Getting 1985).

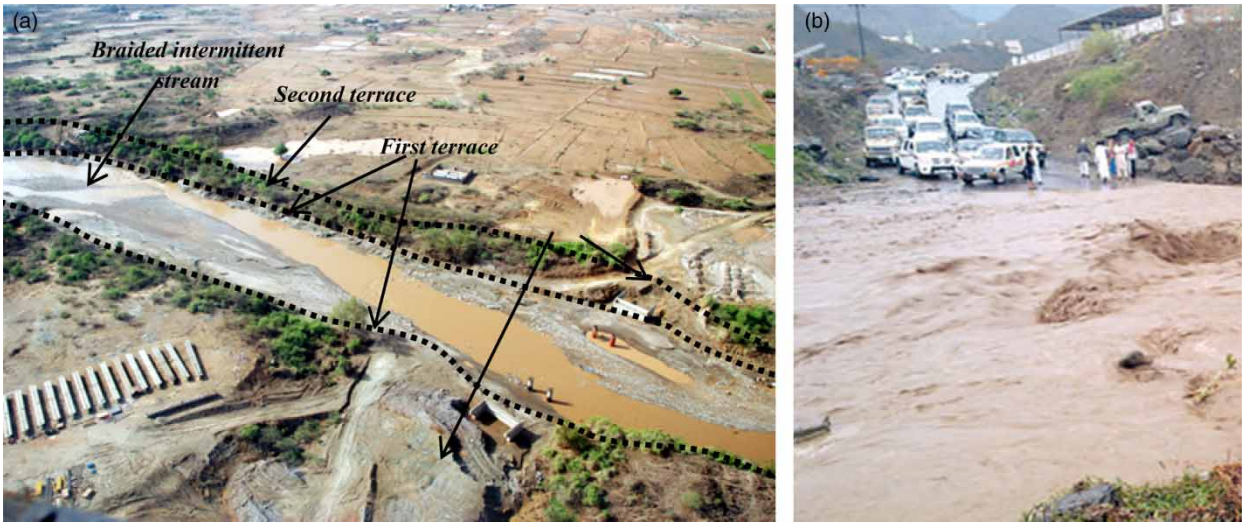

Figure 3 | (a) Aerial photograph of washed up road, Jazan area (29/8/2010), and (b) the road is submerged during a flood, Jazan area (10/8/2003).

STUDY AREA

The study area is located in the Jazan region of southwestern Saudi Arabia, between latitudes 16 °56′–17 °02′N and longitudes 42 °54′–43 °01′E, with an area of 36.7 km^2 (Figure 1). This terrain is characterized by a high relief variability, with ridges and mountain ranges in the eastern part and lowlands in the west. The western part of the study

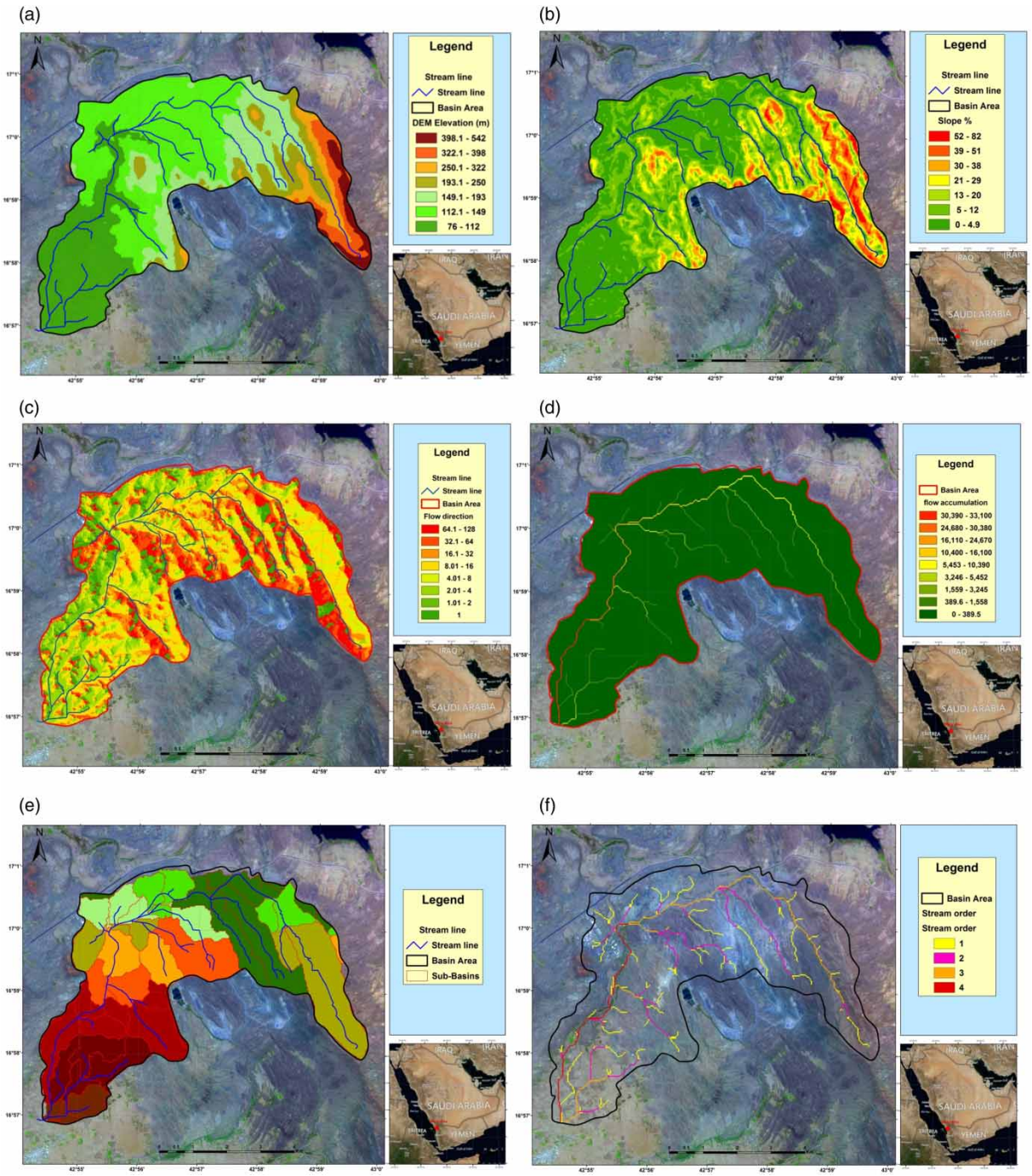

Figure 4 | Wadi Al-Burfi, Jazan area: (a) digital elevation model; (b) slope %; (c) flow direction; (d) flow accumulation; (e) sub-catchment boundaries; (f) stream network orders; (g) estimated morphometric parameters of the third order sub-basins. (*Continued*.)

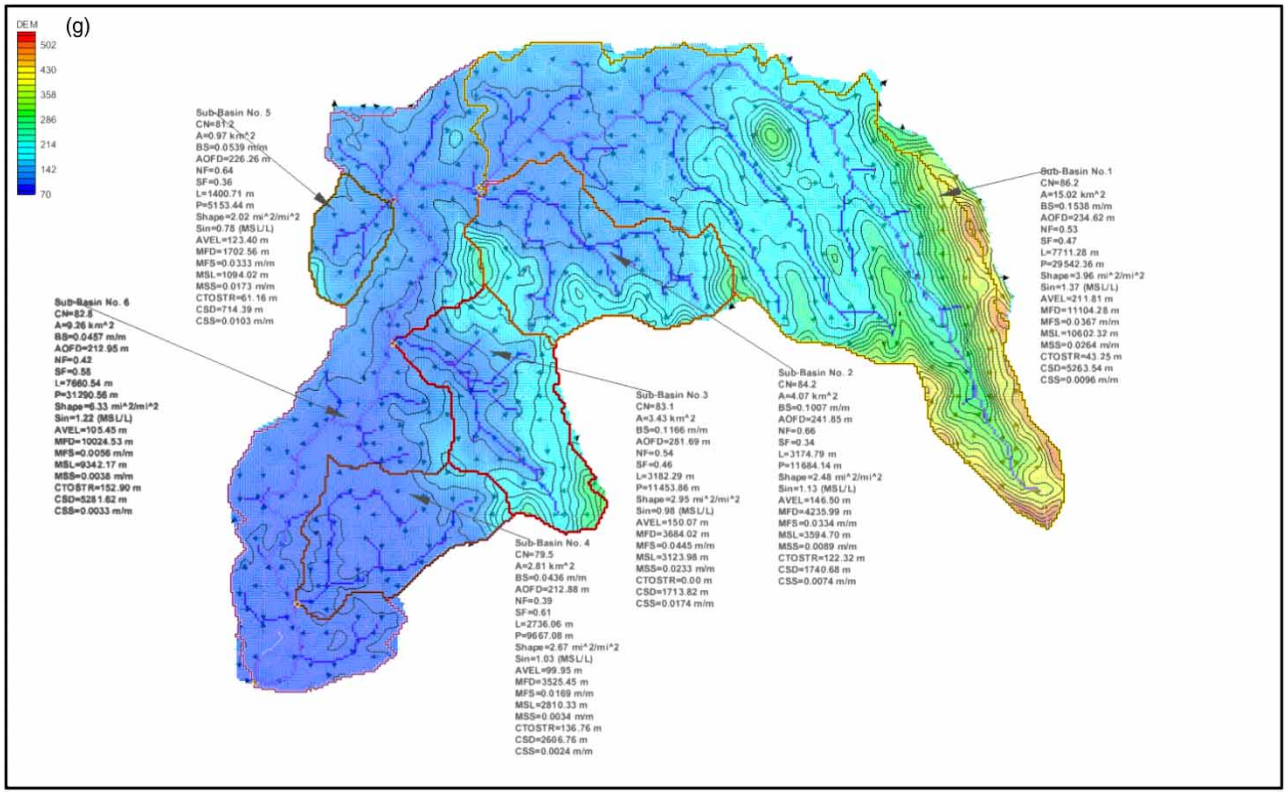

Figure 4 | Continued.

area is a low-lying flat plain with a general slope of $<5^{\circ}$. Toward the east, high undulating terrains are found and the slope increases sharply, reaching 82°.

During the Tertiary period, the Arabian shield was separated from the adjacent African shield by a rift in the Earth's crust that is currently occupied by the Red Sea. The Jazan region is covered by different rock units from the Pre-Cambrian to the Holocene with distinct hydrological properties (Figure 2). In the western part of the basin under study, there is a nearly flat plain covered with Holocene surficial deposits composed of sand and gravel, sand sheets and sand dunes. Further to the east, the Paleozoic sandstone of the Wajid group is exposed, which is composed mainly of medium-coarse grained sandstone, siltstone, and some intercalations of clay. The lower part of the Wajid group is represented by the Dibsiyah and the Sanamah Formations, and the upper part is represented by the Khusayyayn and the Juwayl Formations (Evans *et al.* 1991). Wajid sandstone hosts the most important groundwater resources in southwestern Saudi Arabia, since it has very good hydraulic parameters. Medians of porosities range from 15 to 28%; different permeability measurements show the highest medians of 1,500–2,000 mD for the Khusayyayn Formation and lowest medians of 300–1,400 mD for the Dibsiyah Formation (Al-Ajmi *et al.* 2014). Both the surficial deposits and the Wajid sandstone have low runoff potential and high infiltration rates, even when thoroughly wetted (Group *B*). They have a moderate rate of water transmission (0.15–0.30 in/hr) that permits the infiltration of the rainfall and runoff to the shallow aquifer. In the central part of the basin, the Tertiary basement rocks of moderately weathered, dark green grey alkali-olivine basalts (Harrat) are exposed (Figure 2), sometimes covered with a thin layer of clay. Since the basalt is fine-grained and contains olivine, pyroxene, and calcium-rich plagioclase feldspar, it weathers rapidly and produces clay minerals. These rocks represent Group *C*, since they have low infiltration rates when thoroughly wetted, and a low rate of water transmission (0.05–0.15 in/hr). This increases the generation of storm runoff and decreases infiltration to the aquifer.

The Jazan region has a subtropical, low-latitude, arid, hot desert climate. The annual average rainfall of Abu Arish (an urban part of the study area) does not exceed 211 mm. The terrain variability plays a significant role in the spatial distribution of rainfall, since the rainfall events are not evenly distributed spatially and temporally. The most distinctive features of these convective rainfalls are: local distribution, short durations, and high intensities. Recently, flash flood events on 10/8/2003, 30/8/2010, 30/7/2012, and 23/7/2013 have revealed the inadequacy of current mitigation measures in place to deal with flash floods. Several municipal streets were flooded and fatalities occurred when a number of vehicles drifted in the flow (Figures 3(a) and 3(b)). The gullying of sediments from the abandoned fluvial terraces on the hill slopes clogged the drainage systems and showed the limits of their capacity. This clogging may lead to changes in the flash-flood flow paths, particularly in these braided alluvial channel areas.

MATERIALS AND METHODS

Several inputs of rainfall data, remote sensing data, and hydro-morphometrical measurements, along with DEM analyses and fieldwork, were used to estimate the various hydrological parameters (Scipal *et al.* 2005; Milzow *et al.* 2009). The available data of rainfall–runoff modeling were gathered and processed; such as those of precipitation, terrain analyses, land-use, and wadi hydrogeometric roughness characteristics, which were verified during on-site visits. These different data categories were integrated into GIS to develop a hydrological model for a typical arid land catchment.

Detailed morphometric characteristics of the catchment area were derived from the analysis of the 30 m resolution ASTER DEM (ASTER GDEM Validation Team 2011). ArcGIS-10, Arc-Hydro (ESRI Inc. 2012), and the correlated Topographic Parameterization Program (TOPAZ) of WMS-8.3

Table 1 | Characteristics of the main and third order sub-basins and their channel networks

	Sub-basin No. 1	Sub-basin No. 2	Sub-basin No. 3	Sub-basin No. 4	Sub-basin No. 5	Main basin
Area (km^2)	15.02	4.07	3.43	2.81	0.97	36.70
Length (km)	11.10	4.24	3.68	3.53	1.71	20.28
Perimeter (km)	29.54	11.68	11.45	9.67	5.15	47.76
Minimum elevation (m asl)	112	112	101	90	112	90
Maximum elevation (m asl)	497	255	299	200	167	497
Mean elevation (m)	212	147	150	100	123	159
Height range (m)	385	143	198	110	55	407
Slope (m/m)	0.15	0.10	0.12	0.04	0.05	0.11
Average overland flow (m)	235	242	282	213	226	226
North-facing aspect	0.53	0.66	0.54	0.39	0.64	0.51
South-facing aspect	0.47	0.34	0.46	0.61	0.36	0.49
Shape factor	3.96	2.48	2.95	2.67	2.02	2.81
Elongation ratio	0.57	0.72	0.66	0.69	0.80	0.34
Sinuosity factor	1.37	1.13	0.98	1.03	0.78	1.99
Maximum flow distance (m)	11,104	4,236	3,684	3,226	1,703	20,313
Maximum flow slope (m/m)	0.037	0.033	0.023	0.003	0.033	0.022
Maximum stream length (m)	10,602	3,595	3,124	2,810	1,094	19,842
Maximum stream slope (m/m)	0.026	0.009	0.023	0.003	0.017	0.016
Distance from centroid to stream (m)	43.25	122.32	0.00	136.76	61.16	319.27
Centroid to stream distance (m)	5,264	1,741	1,714	2,607	714	11,718
Centroid to stream slope (m/m)	0.009	0.007	0.017	0.002	0.010	0.006

(2010) were used for the integrated analysis of the catchment involving the correlation and verification of topographic maps and DEM. These analyses were carried out to determine the spatially distributed time-area zones of the catchment to simulate the runoff hydrographs under different projected return periods for future storms over the long term. Various methods for channel network delineation and characterization were conducted, including DEM reconditioning, flow accumulation, flow direction, stream definition, sub-catchment definition, DEM slope, and others (Figures 4(a)–4(f)). The raw DEM sinks were removed before being used in hydrological modeling (Mark 1984; Wise 2000). The flow direction was computed by calculating the steepest slope towards the surrounding cells. This flow direction was used to generate the flow accumulation map, which was used to delineate the stream networks to the outlets of the basin. Different threshold values proposed by Djokic *et al.* (1997) were examined to correct the generated flow lines with the actual network using the Landsat-8 and SPOT-5 images verification. The fourth order of the main wadi trunk was computed to attain the hydrologic analysis of the main basin (Figure 4(f)), while the morphometric parameters of the third order sub-basins were estimated to assess the flooding potentialities at this order level, since several small retardation dams could be proposed (Table 1 and Figure 4(g)).

Rainfall analyses were based on reviewing and processing 46 years of historic records for the SA-101 station located at the outlet of the studied basin (PME 2011). Five hypothetical design storms were developed for the events with 5, 10, 25, 50, and 100 year return periods. An intensity duration frequency (IDF) relationship is a mathematical relationship between the rainfall intensity i, the duration d, and the return period T. IDF-curves allow for the estimation of the return period of an observed rainfall event, or conversely, of the rainfall intensity corresponding to a given return period for different aggregation times. The equations of Gumbel's method were used to perform the best probability distribution and the calibrated equation for IDF curves.

Landsat-8 (2015) and SPOT-5 satellite images (2010) were analyzed and classified using Erdas Imagine (2010) and ArcGIS (ESRI Inc. 2012) to delineate the different land-use types using the maximum likelihood method. This was verified

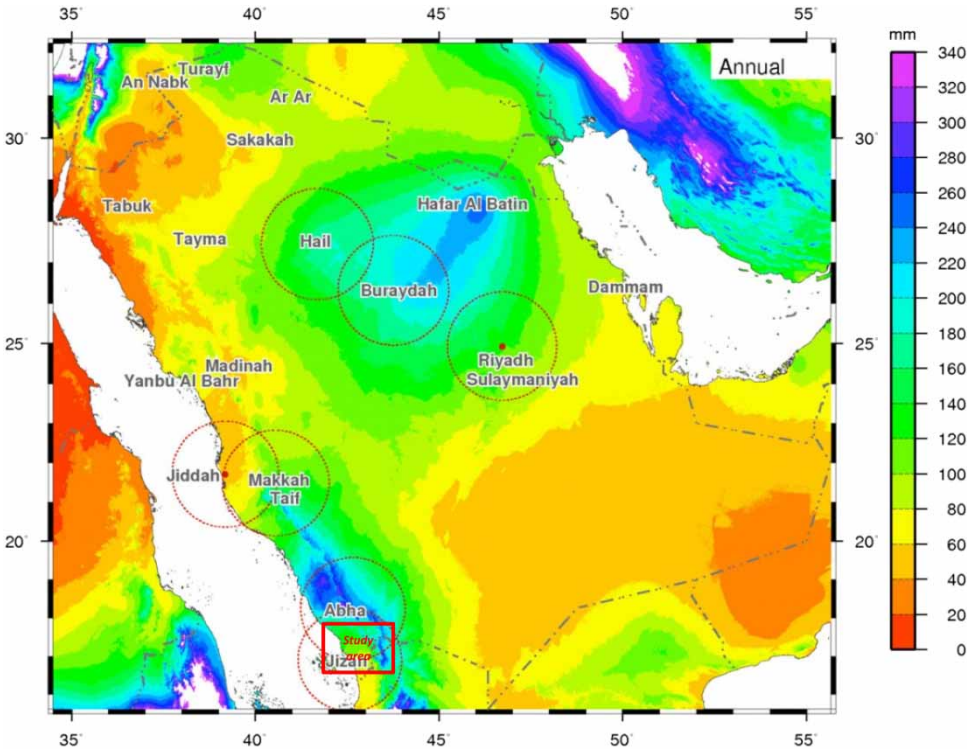

Figure 5 | Annual rainfall of Saudi Arabia (National Center for Atmospheric Research 2008).

using a geological map and field investigations to validate and update the derived GIS layers. The SCS runoff CN method was used to abstract the total rainfall hyetograph into the effective rainfall hyetograph. Also it was used to model the hydrographs at each sub-catchment outlet by relating hydrograph characteristics to catchment parameters. A distribution curve was used which resembles the SCS Type II curve, and this type of distribution curve has been used in rainfall studies in arid areas including Saudi Arabia (Wheater & Bell 1983). The SCS CN infiltration method was used to identify the effective rainfall. This approach requires estimating a CN of the land-use and soil hydrologic properties. The relationships between rainfall depth (P), and runoff depth (Pe) are identified in the SCS method (USDA 1986). The lag time (Tl), time of concentration (Tc), time to peak (Tp) and maximum of discharge parameters are calculated to perform the calculation of peak discharge and quantity of storm runoff.

$$P_e = \frac{(p - 0.2S)^2}{(P + 0.8S)}, \text{ For } P > 0.2\,S;\ else\ P_e = 0 \tag{1}$$

$$S = \left(\frac{25400}{CN}\right) - 254 \tag{2}$$

$$I_a = 0.2\,S \tag{3}$$

$$S = \left(\frac{1000}{CN}\right) - 10 \tag{4}$$

where Pe is the surface runoff depth (mm), P is the precipitation depth (mm), S is the soil retention (mm), Ia is the initial loss (mm), and CN is the curve number.

The hydrologic analysis was used to derive the natural flood flow paths and estimate the peak flow rates at designated locations using the HEC-HMS model. This model was selected for several reasons: (1) model availability and structure, (2) data availability, and (3) model applicability in arid catchments. The HEC-HMS model includes three main components: a basin model, a meteorological model, and control specifications. This model was conducted as a function of the catchment's descriptive parameters (morphometric parameters, soil type, and land-use), antecedent moisture conditions, and the average of the maximum daily rainfall for each year (Mishra & Singh 2004). The SCS-CN loss rate method was used to compute the stream-flow volume. The SCS unit hydrograph method was used to determine transformation and recession. Hydrographs were identified and then used to feed into the peak flow estimations under different rainfall events. They were drawn and routed to the main catchment outlets based on appropriate wadi dimensions and roughness. At Wadi Al-Maayen, a tributary of Wadi Al-Burdi, a single rainfall–runoff event data set on 30/07/2012 was used to calibrate the HEC-HMS model (rainfall was 53 mm/day). This calibration was performed to reach the best fit between observed and simulated values by applying different CNs in the HEC-HMS simulated model. HEC-HMS offers both automated and manual calibration (Scharffenberg 2013), and in this study, the automated calibration procedure was used. The Nash–Sutcliffe efficiency (Ef) method was utilized to quantify the goodness-of-fit between the modeled stream flow and observed records:

$$E_{\mathrm{f}} = 1 - \frac{\sum (q_i - \hat{q}_i)^2}{\sum (q_i - \bar{q}_i)^2} \tag{5}$$

where q_i is the observed stream flow, $\hat{q}_i$ is the simulated stream flow, and $\bar{q}_i$ is the mean value of observed stream flow.

A sensitivity analysis was carried out to study the behavior of the modeled stream flow with respect to the change of parameter values. This method is useful for complex hydrological models that involve a large number of parameters (Liu & Sun 2010). In addition, it is particularly important for an arid catchment to identify the local controlling parameters. The relative sensitivity analysis (R) was carried out according to the equation of Al-Abed *et al.* (2005):

$$R = [((FY2 - FY1)/Y)/((FX2 - FX1)/X)] \tag{6}$$

where $FY1$ is the output result for the original case, $FY2$ is the output result for the new parameter with a specific change, $FX1$ is the original parameter value, and $FX2$ is the new parameter value with the specific change.

RESULTS AND DISCUSSION

In the study area, the rainfall analysis shows that local distribution, short durations, and high intensities are the most

Table 2 | Statistics of the 24 hr rainfall depths (mm) at Abu Arish metrological station

Number of observations	**46**		
Minimum (*Max*)	6.90	Median ($\tilde{x}$)	38.5
Maximum (*Min*)	126.00	Coefficient of variation (*Cv*)	0.54
Mean ($\bar{x}$)	41.10	Skewness coefficient (*Cs*)	1.42
Standard deviation (σ)	22.30	Kurtosis coefficient (*Ck*)	5.82

Table 3 | Twenty-four hour rainfall depths estimated for different return periods at Abu Arish metrological station

Return period (years)	**5**	**10**	**25**	**50**	**100**
24 hr rainfall height (mm)	57.18	70.23	86.76	98.95	111.13

distinctive features of these rainfall events (Figure 5). The annual average rainfall in the Abu Arish area does not exceed 211 mm (Tables 2 and 3). Temporally, most rainfall events occur in April and between July and October. Spatially, the eastern mountainous area has more rainfall than the western plain area, and the sloping land of the eastern area causes a sharp drop in the watershed's ability to conserve water, especially in the eastern part as ground slopes vary between 52 and 82° (Figure 4(b)). Statistical frequency analyses of 46 years' (1963–2009) available data show a highly erratic trend in rainfall patterns, with both positive and negative deviations from the mean value (Tables 2 and 3, and Figures 5 and 6). From these analyses, projections were made for annual 1 day maximum rainfall, and 2–5 day consecutive maximum rainfall, corresponding to return periods. The area has a recorded maximum rainfall of 126 mm (Tables 2 and 3, and Figures 6 and 7). IDF curves were developed using Gumbel frequency analysis techniques, where *c*, *m*, and *e* parameters are 411.10, 81.0, and 0.76, respectively (Figure 7). The 10 minute rainfall intensity varies between 80 and 160 mm/hr for 2 and 100 year return periods. IDF curves like these are a useful aid when designing drainage works for any project and facilitate the design of safe and economical flood control measures.

Based on the hydrologic soil groups, the CN values were calculated using an unsupervised classification followed by a supervised classification of a 2010 SPOT-5 image (before urbanization) and a 2015 Landsat-8 image (after urbanization). These values were validated using field check activities. Reasonable results were obtained from the classification, where the Kappa coefficients of Congalton (1991) showed an average commission of 92% and 93% for the urban, soil, rock, and vegetation areas. Based on this classification, the infiltration rates into the catchment were assigned to groups *B* and *C* (Table 4 and Figures 2, 8(a) and 8(b)). The percent of imperviousness for each subbasin is estimated based on current and proposed land-use types (Figures 8(a) and 8(b)). As per the NRCS CN tables and other relevant data, a composite CN of 81.59 is assumed for the 2010 land-use map. However, Harrat (basalt rocks),

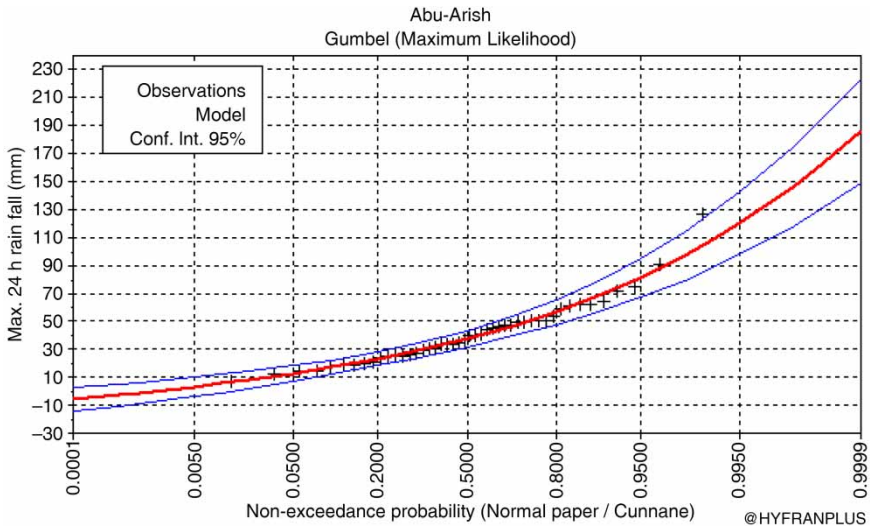

Figure 6 | Twenty-four hour rainfall depths and cumulative probability (Gumbel) at Abu Arish.

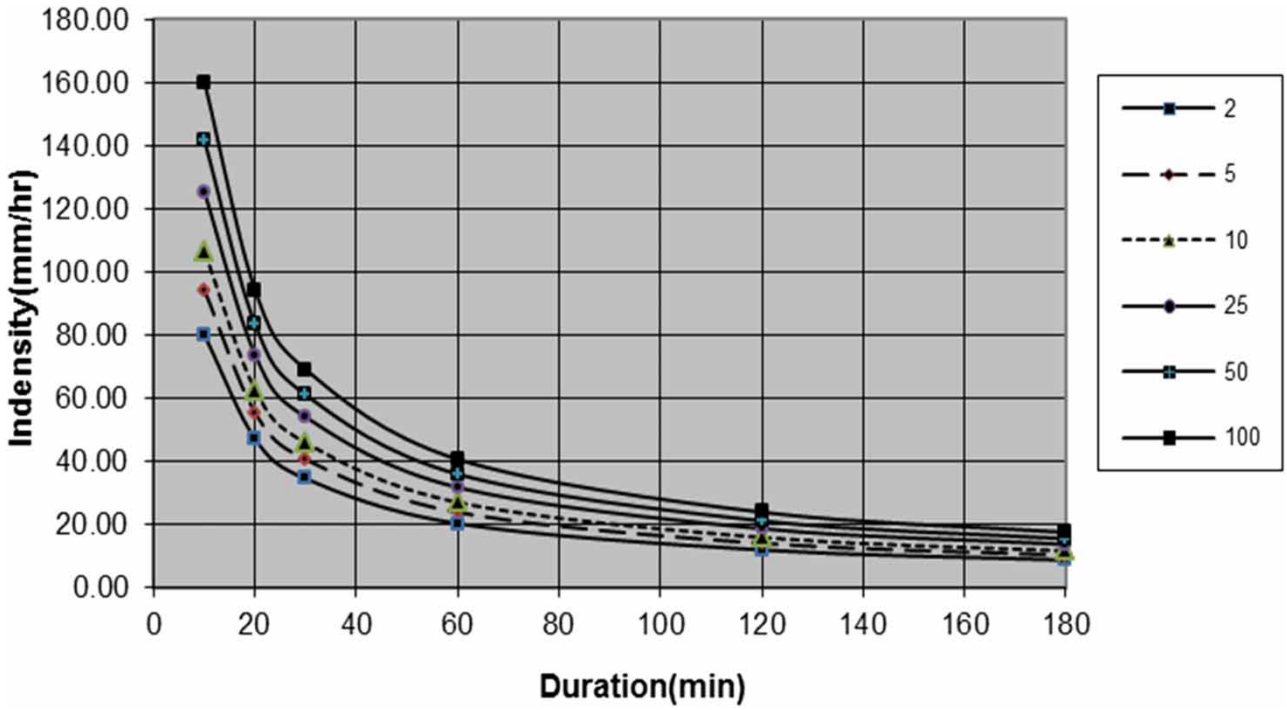

Figure 7 | IDF curves computed by Gumbel method at Abu Arish area (2–100 years).

sand and gravel, vegetation, and fine barren sandy and silty soils cover the area (Table 4). Urbanization is taking place rapidly in the southwestern part of the studied watershed. Accelerated urban expansion in 2015 is causing changes in catchment land-use, increasing the composite *CN* to 83.71. Comparison of the two successive land-use maps (2010–2015) shows that urbanization increased by 8% of the total area (Table 4 and Figures 8(a) and 8(b)).

Table 4 | Calculations of the weighted CN in the study area (2010 and 2015)

		Land-use/cover	Area (*A*) km^2	Curve number (*CN*)	A*CN	W.CN
2010	1	Harrat (basalt)	17.12	86	1472.32	
	2	Sand and gravel	9.12	76	693.12	
	3	Vegetated area	7.17	78	559.26	
	4	Fine sand and silty soil	3.29	82	269.78	
		Σ	36.7		2,994.48	81.59
2015	1	Harrat (basalt)	16.64	86.00	1,431.04	
	2	Sand and gravel	6.32	76	480.32	
	3	Vegetated area	6.14	78	478.92	
	4	Fine sand and silty soil	3.08	82	252.56	
	5	Urban-up area	4.52	95	429.40	
		Σ	36.70		3,072.24	83.71

The morphometric parameters of the main Wadi Al-Burdi basin and its third order sub-basins were computed (Figures 9(a)–9(c) and Table 1) with emphasis on its implication for hydrologic processes. The wadis dissecting the mountain ranges to the east are characterized by complex and interlocking patterns reflecting the morphotectonic evolution of these drainage basins, where the paleo-channels flow in different directions from the contemporaneous flow pathways (Figures 4(a)–4(f)). The textural dissection of Wadi Al-Burdi was considered to be low as drainage density and stream frequency are low, since the study area is covered with highly resistant hard basement rocks, making it susceptible to flooding (Figures 2 and 4(a)–4(f)). The main basin of Wadi Al-Burdi has an area of 36.7 km^2, and a mean basin elevation of 166.6 masl. It has a moderate

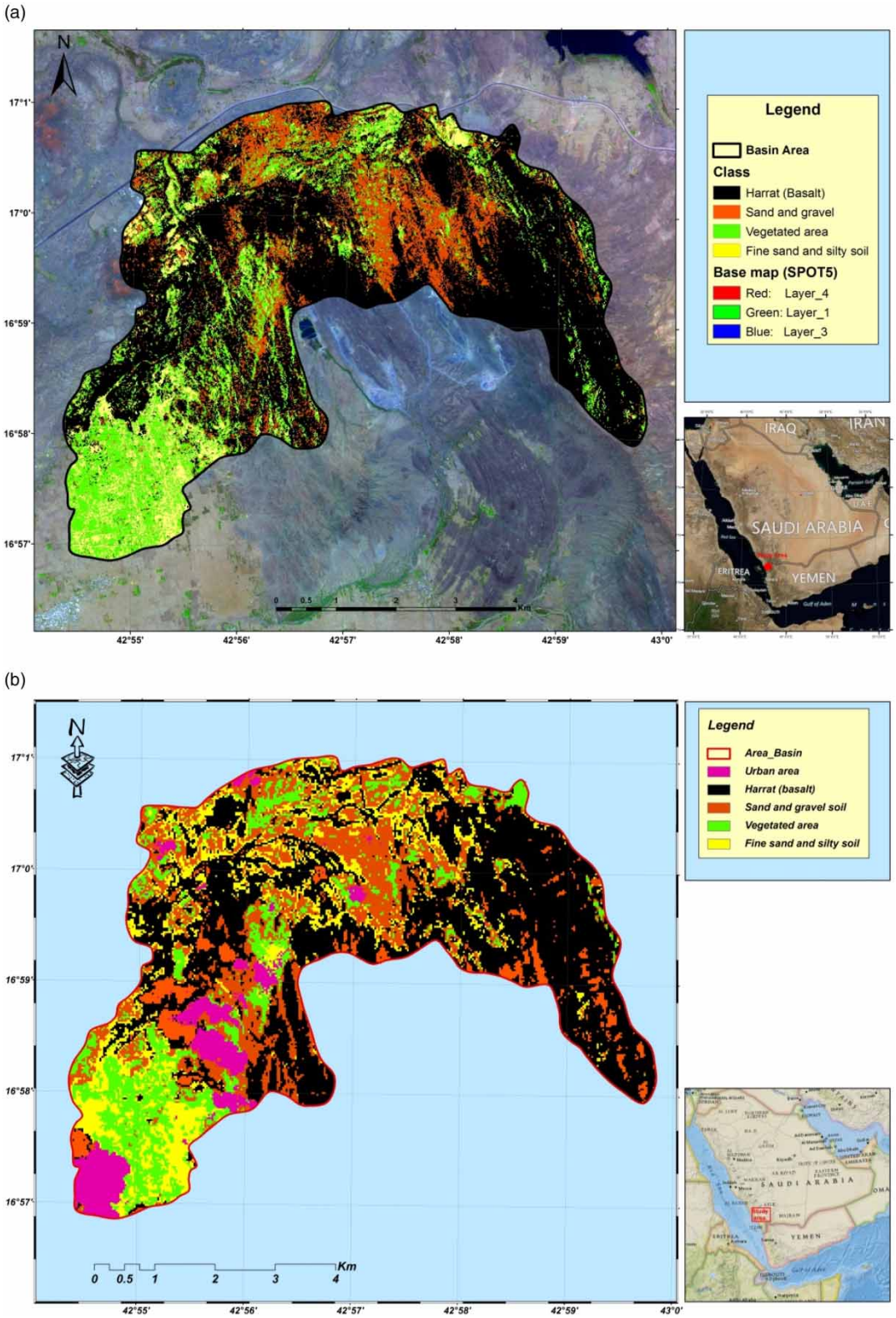

Figure 8 | (a) Land-use map of the study area classified according to: (a) SPOT-5 Satellite image (2010); (b) Landsat-8 Satellite image (2015).

Table 5 | Estimated morphometric and storm time parameters of the third order sub-basin and the main basin

		Area (*A*) km^2	Watershed length (*L*) km	Watershed slope (%)	Average overland slope	Lag time (*Tl*) min.	Time of concentration (*Tc*) min.	Time to peak (*Tp*) min.
2010	Sub-basin No. 1	15.02	11.10	15.38	0.037	82	85	170
	Sub-basin No. 2	4.07	4.24	10.07	0.033	47	42	143
	Sub-basin No. 3	3.43	3.68	11.66	0.045	39	34	125
	Sub-basin No. 4	2.81	3.53	4.36	0.017	62	47	149
	Sub-basin No. 5	0.97	1.71	5.39	0.033	31	21	117
	Main basin	36.70	20.28	10.49	0.022	161	165	251
2015	Sub-basin No. 1	15.02	11.10	15.38	0.037	77	78	157
	Sub-basin No. 2	4.07	4.24	10.07	0.033	44	38	123
	Sub-basin No. 3	3.43	3.68	11.66	0.045	36	31	115
	Sub-basin No. 4	2.81	3.53	4.36	0.017	57	43	136
	Sub-basin No. 5	0.97	1.71	5.39	0.033	29	19	108
	Main basin	36.70	20.28	10.49	0.022	149	150	235

relief with an average slope percent of 10.6. Its shape is relatively elongated with a length of 20.3 km. It has a shape factor of 3.1 (Table 1). The basin sinuosity factor is 1.98, which suggests tectonics as the major factor influencing the basin's development, which is well correlated with the geologic structures (Figures 2 and 4). The lag time, time of concentration, and time to peak of the third order sub-basins of Wadi Al-Burdi were computed before and after urbanization (2010 and 2015). They were estimated for the main basin to be 161 min, 165 min, and 251 min for the 2010 land-use map, and 149 min, 150 min, and 235 min for the 2015 land-use map, respectively (Table 5). This reflects that the size, slope, shape, surface roughness, and land-use of the contributing basin have a direct influence on runoff.

The hydrologic parameters of the studied basin were computed using the HEC-HMS model. The areas, lag time, and predicted peak discharge rates, along with the volumes of rainfall, runoff, and abstraction losses were computed. Also the predicted hydrographs were estimated (Figures 10(a)–10(f)). One of the main benefits of deriving this model is to estimate different hydraulic parameters in ungauged watersheds; therefore model validation is essential. For this purpose, peak flow rates are estimated using the derived model, and compared with the observed values (Figure 11). An accuracy test was carried out to assess the ability of the relationship to predict peak flow rate, resulting in a Nash–Sutcliffe model efficiency coefficient of 86%. The relative sensitivity analysis was done by adjusting different parameter values in the HEC-HMS model. After running the models repeatedly, the simulated flow results were compared with monitored values at each change of parameters. Hydrologic influences of the ground surface are found to have a major impact on the timing, location, and severity of flash flooding. The most sensitive parameters in the HEC-HMS model are the *CN* with an average of 2.5, while the imperviousness relative sensitivity value was 3.3. The rest of the parameters in the HEC-HMS model were shown to have a weak effect on the modeled outputs.

The susceptibility of the Wadi Al-Burdi basin to flash floods is high due to the scarcity of stream meanders, steep slopes, and low surface roughness. The estimated peak flow rate for 2–100 year return periods of the main basin in 2010 vary between 63.7 and 150.3 m^3/s (Table 6 and Figure 12(a)). The estimated peak flow rate for the same return periods in 2015 varies between 77.4 and 171.7 m^3/s (Table 6 and Figure 12(b)). The comparison between the peak flow rates of 2010 and 2015 shows distinctive increasing of the flash flood peaks by 14–22%. This is due to the nearly 8% increase in urbanization activities (Figure 13 and Tables 4 and 6). The model results show rapid urbanization adversely affects the hydrological processes, since the sprawl on the alluvial channels is significant. This reduces the infiltration into the underlying alluvium and increases the runoff and leads to higher flood peaks and volumes even for short duration low intensity rainfall. The flash floods are formed and concentrated

(a)

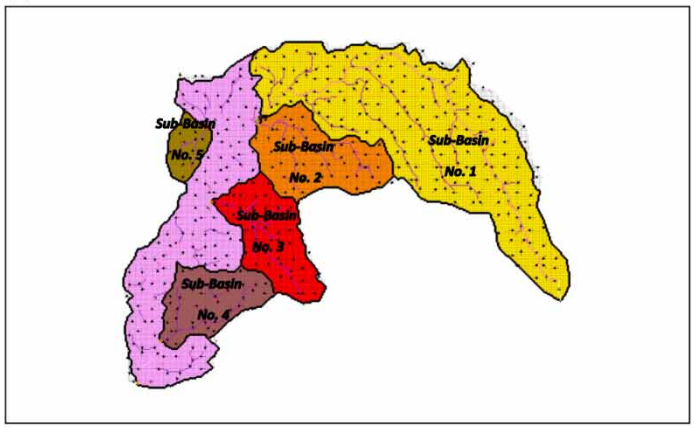

(b)

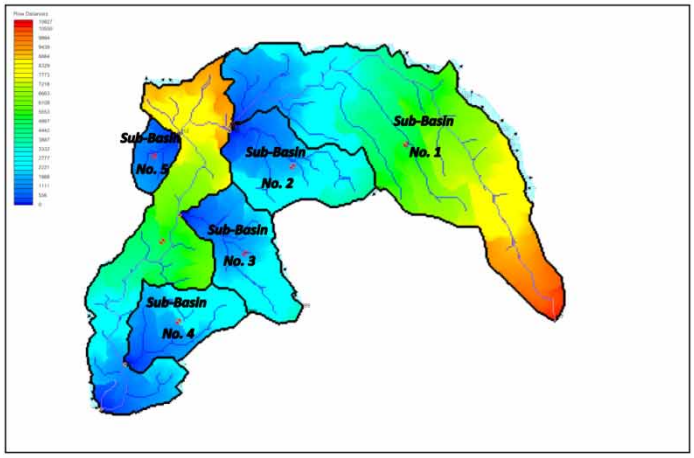

(c)

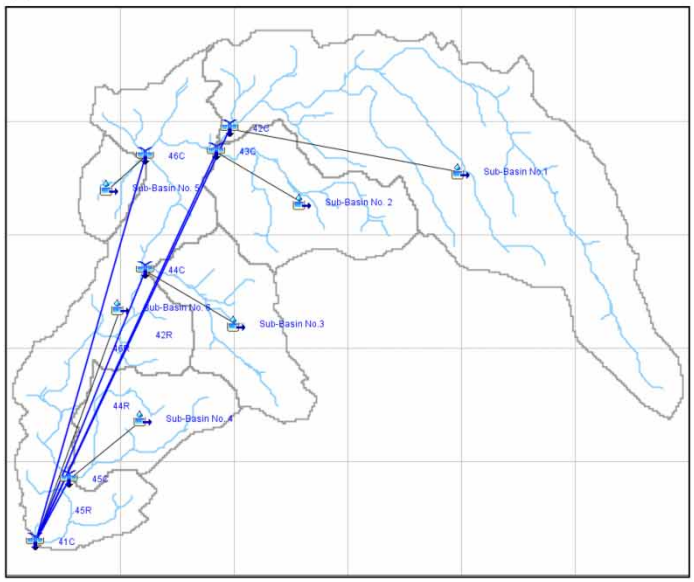

Figure 9 | Wadi Al-Burdi, Jazan area: (a) the selected third order sub-basins for the hydrologic modeling; (b) sub-Basin flow distances; (c) basin model.

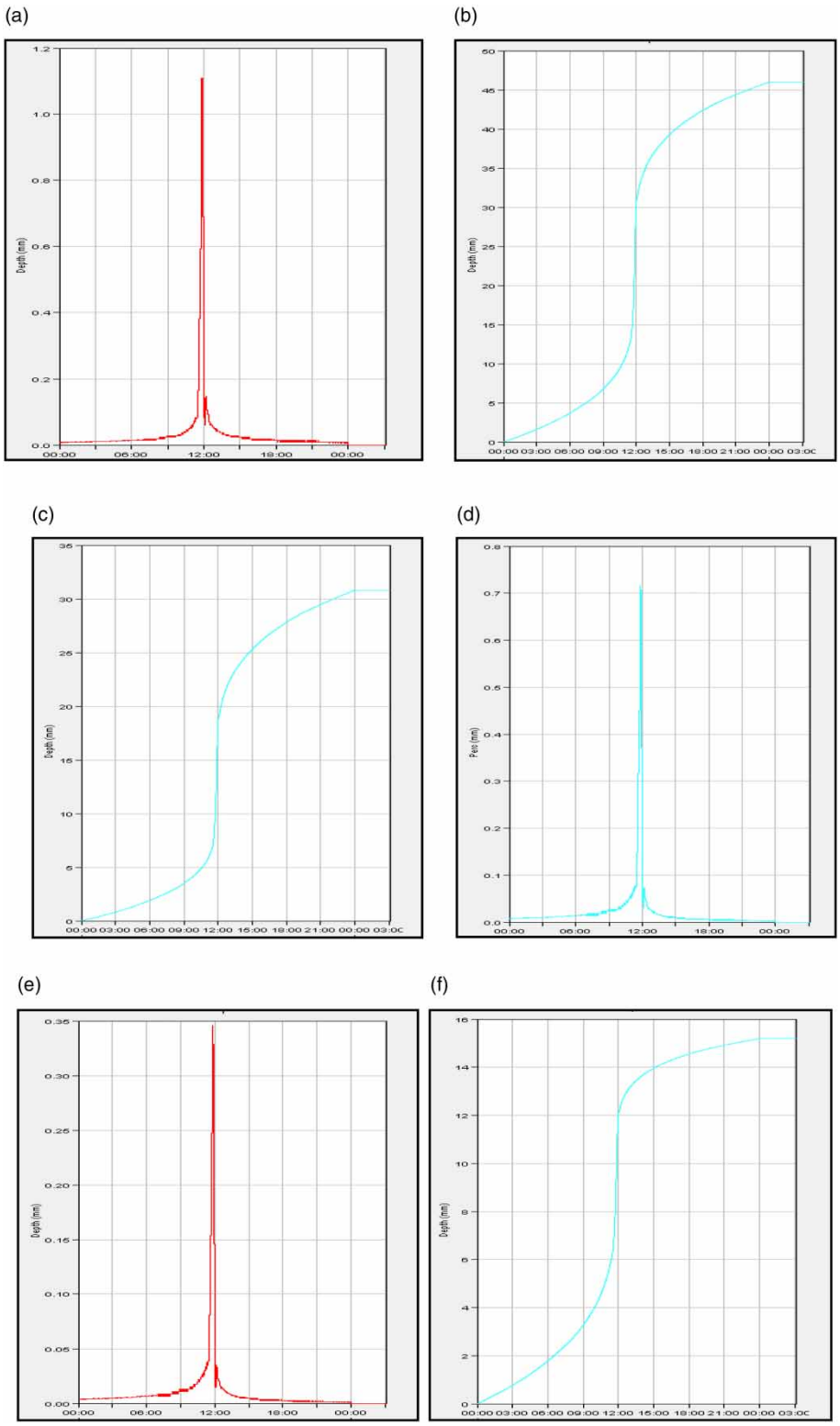

Figure 10 | Twenty-four hour computations in mm: (a) precipitation; (b) cumulative precipitation; (c) cumulative excess precipitation; (d) soil infiltration; (e) precipitation loss; (f) cumulative precipitation loss.

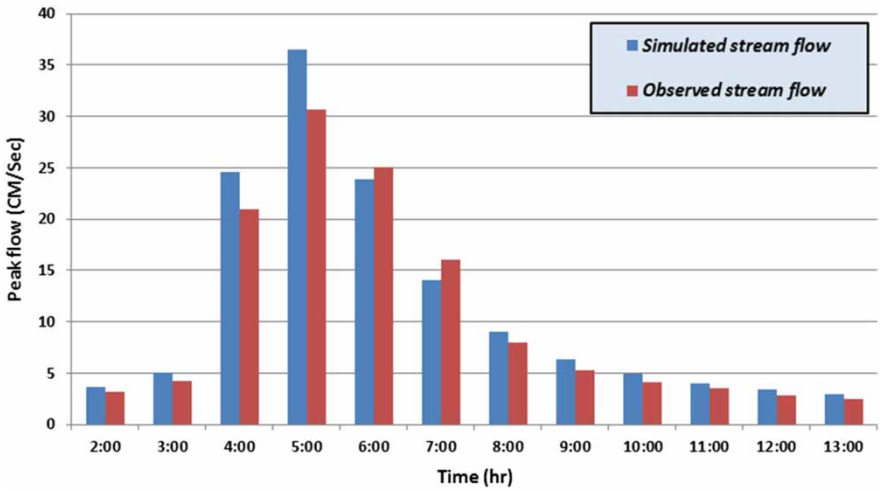

Figure 11 | Wadi Al-Maayen catchment observed vs. simulated stream flow hydrographs for the calibration (30/07/2012) using HEC-HMS.

within a short time; however, higher precipitation intensity can result in more runoff as the soil cannot absorb the water quickly enough. The high peak of these floods presents a potential threat to both infrastructure and human life in this area.

The recommended management strategies for these flash floods include: (1) the construction of several small dams at the outlet of the third order sub-basins, (2) rainfall-sewage systems, and (3) conveyance culverts (in the upper part of the catchment) and levees alongside the wadis to transfer the flows into Jazan dam lake (Figure 1). Additionally, the considerable quantity of fresh water in this arid region could serve as a good water supply for the local inhabitants. Indeed, the total runoff volumes are computed to vary between 1.6 and 3.4 million m^3 (Table 6). Regrettably, almost all of this water is lost due to the spreading of the meandering wadi channel and the consequent high evapotranspiration rates. It is recommended that this renewable water resource could be used to recharge groundwater through wells employing natural downward percolation or even through injection wells.

CONCLUSIONS

In arid areas, reliable prediction of runoff is difficult to achieve for ungauged basins. Peak discharge of flash floods in ungauged catchments could be estimated efficiently by coupling GIS and remote sensing tools with hydrologic modeling. This approach will help to further

Table 6 | Estimated rainfall, direct runoff and peak flows of the main basin

		5 years	10 years	25 years	50 years	100 years
2010	Rainfall max 24 hr (mm)	57.18	70.23	86.76	98.95	111.13
	Total precipitation (m^3)	2,098,500	2,577,400	3,184,100	3,631,500	4,078,500
	Total loss (mm)	19.68	21.60	23.48	24.59	25.53
	Direct run off (mm)	37.50	48.63	63.28	74.36	85.60
	Total run off (million m^3)	1,376,100	1,784,900	2,322,500	2,729,000	3,141,600
	Peak flow rate (m^3/sec)	63.7	83.7	110.1	130.0	150.3
2015	Total loss (mm)	14.42	15.69	16.92	17.64	18.25
	Direct run off (mm)	42.76	54.54	69.84	81.31	92.88
	Total run off (million m^3)	1,569,300	2,001,600	2,563,000	2,983,900	3,408,800
	Peak flow rate (m^3/sec)	77.4	99.5	128.3	149.9	171.7

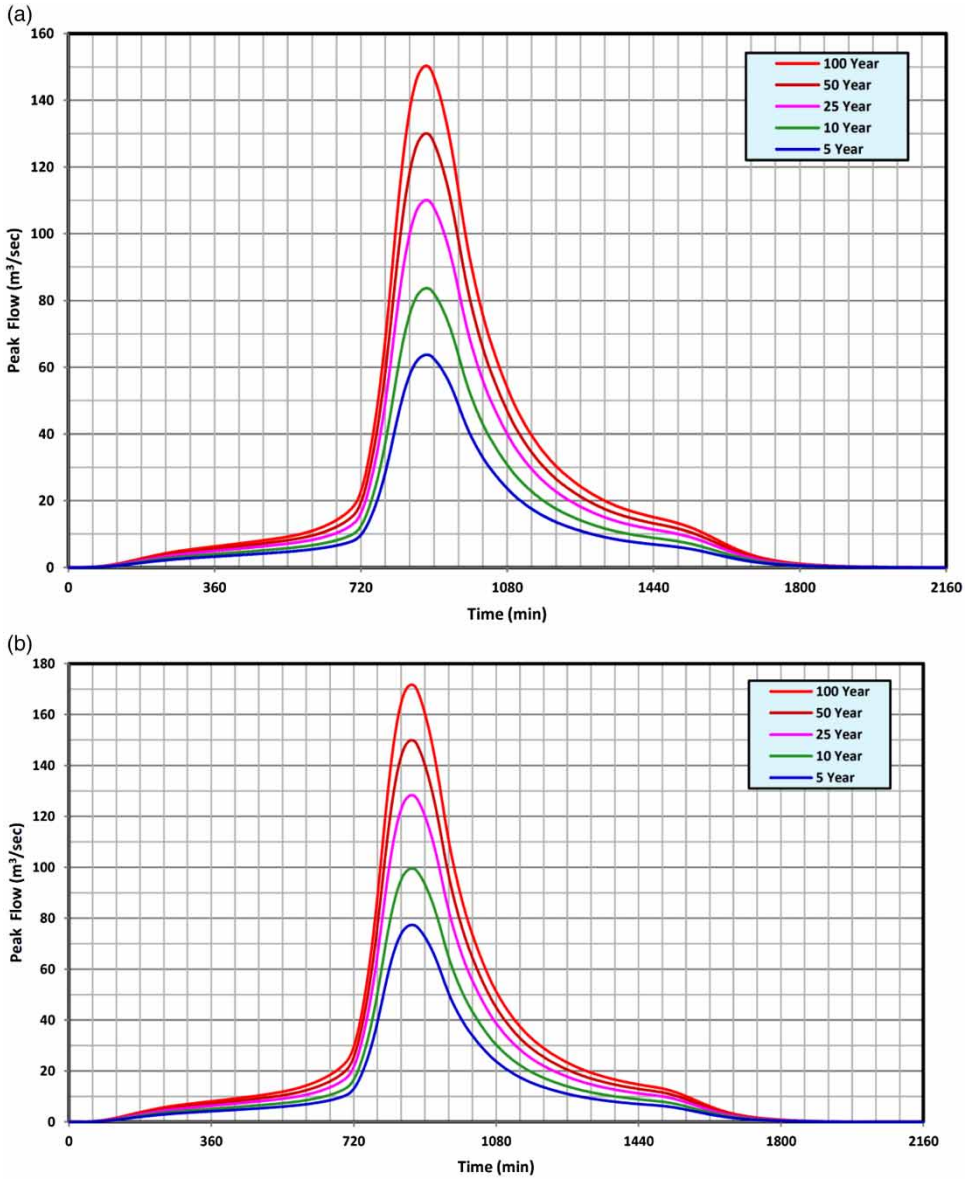

Figure 12 | (a) Estimated peak flows for 5–100 year events Wadi Al-Burdi main basin: (a) before urbanization; (b) after urbanization.

improve our understanding of flash flood processes in such arid regions. Hydrologic influences and urbanization have a major impact on the timing, location, and severity of flash flooding. As per the SCS tables and other relevant data, a composite CN of 81.59 is assumed for the 2010 land-use map. Urbanization is taking place rapidly in the southwestern part of the studied watershed. Accelerated urban expansion in 2015 caused changes in catchment land-use, increasing the composite *CN* to 83.71. The areas, lag time, and predicted peak discharge rates, along with the volumes of rainfall, runoff, and abstraction losses were computed. The calibration of the HEC-HMS model is an essential step to reduce prediction errors for a single storm event. The estimated and observed stream flow volumes of a single event are close enough to assume the applicability of the HEC-HMS model approach for the arid area. The susceptibility of the Wadi Al-Burdi basin to flash floods is high due to the scarcity of stream

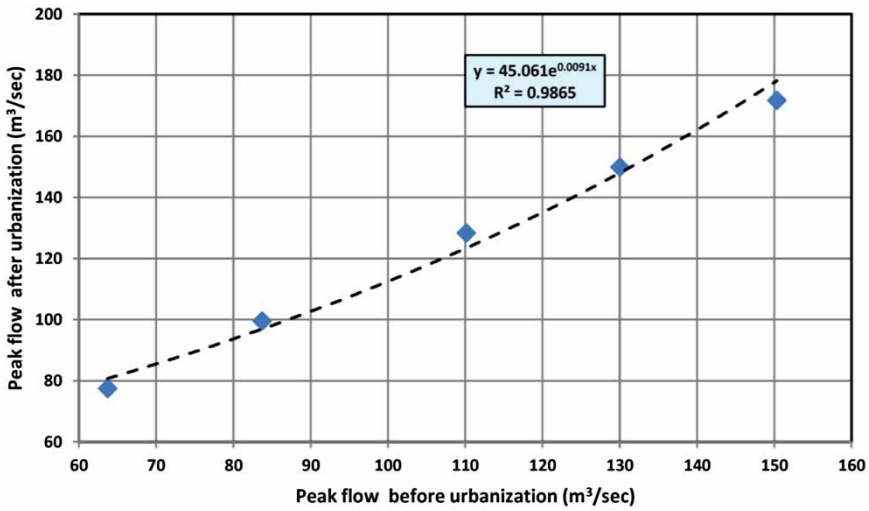

Figure 13 | The relation between the flood peak flow before and after urbanization.

meanders, steep slopes, and low surface roughness. Rainfall estimations from different return periods are identified and probable maximum floods of the sub-basins are also estimated for different return periods between 2010 and 2015. Due to encroachment of the flood plain areas, the presence of several structures, and the absence of proper regulations for maintenance, the flood intensity is increased. Comparison of the two successive land-use maps (2010–2015) shows that urbanization increased by 8% of the total area. The model results show rapid urbanization adversely affects the hydrological processes, since the sprawl on the alluvial channels is significant. This reduces the infiltration into the underlying alluvium and increases the runoff, leading to higher flood peaks and volumes even for short duration low intensity rainfall, therefore increasing the potential threat to both lives and property. The construction of several small dams is recommended at the fingertip channels at the outlets of the third order sub-basins, in order to retain a considerable amount of water and sediments. Not only will these dams decrease the flood hazards, but they could also serve as a recharge source to the underlying alluvium aquifer. This flood water could be used to cover a considerable amount of the region's water supply, and be utilized to fulfill part of the increasing water demand due to the current high population growth and expected economic development in this arid area.

ACKNOWLEDGEMENTS

The author wishes to express his gratitude to the editor, the reviewers and Dr David Jalajel for their valuable comments and assistance in revising the manuscript. This project was financially supported by the Vice Deanship of Research Chairs at King Saud University.

REFERENCES

Al-Abed, N., Abdulla, F. & Abu Khyarah, A. 2005 GIS-hydrological models for managing water resources in the Zarqa River basin. *Environ. Geol.* **47**, 405–411.

Al-Ajmi, H., Hinderer, M., Rausch, R. & Schüth, C. 2014 Matrix versus fracture permeability in a regional sandstone aquifer, (Wajid sandstone, SW Saudi Arabia). *Grundwa* **19** (2), 151–157.

Al-Ghamdi, K., Elzahrany, R., Mirza, M. & Dawod, G. 2012 Impacts of urban growth on flood hazards in Makkah City, Saudi Arabia. *Int. J. Water Res. Environ. Eng.* **4**, 23–34.

Al-Khalaf, A. 1997 Predicting short-duration, high-intensity rainfall in Saudi Arabia. MS Thesis, Faculty of the College of Graduate Studies, King Fahad University of Petroleum and Minerals, Dhahran, KSA, 196 p.

Al-Qurashi, A., McIntyre, N., Wheater, H. & Unkrich, C. 2008 Application of the Kineros2 rainfall-runoff model to an arid catchment in Oman. *J. Hydrol.* **355** (1–4), 1–214.

ASTER GDEM Validation Team 2011 http://www.jspacesystems.or.jp.

Blank, H. & Getting, M. 1985 Reconnaissance geologic map of the Jizan Quadrangle, sheet 16/42 B, Kingdom of Saudi Arabia. US Geological Survey. Open-File Report 85–724.

Borga, M., Boscolo, P., Zanon, F. & Sangati, M. 2007 Hydrometeorological analysis of the August 29, 2003 flash flood in the eastern Italian Alps. *J. Hydrometeorol.* **8** (5), 1049–1067.

Campana, N. & Tucci, E. 2001 Predicting floods from urban development scenarios: case study of the Diluvio basin, Porto Alegre, Brazil. *Urban Water* **3**, 113–124.

Chin, A. & Gregory, K. 2001 Urbanization and adjustment of ephemeral stream channels. *Ann. Assoc. Am. Geogr.* **91**, 595–608.

Congalton, R. 1991 A review of assessing the accuracy of classifications of remotely sensed data. *Remote Sens. Environ.* **37**, 35–46.

Cooke, R., Brunsden, D., Doornkamp, J. & Jones, D. 1982 *Urban Geomorphology in Drylands*. Oxford University Press, Oxford.

Dawod, G. & Koshak, N. 2011 Developing GIS-based unit hydrographs for flood management in Makkah Metropolitan Area, Saudi Arabia. *J. Geogr. Inform. Syst.* **3** (2), 153–159.

Dawod, G., Mirza, M. & Al-Ghamdi, K. 2011 GIS-based spatial mapping of flash flood hazards in Makkah city, Saudi Arabia. *J. Geogr. Inf. Syst.* **3** (3), 217–223.

Djokic, D., Ye, Z. & Miller, A. 1997 Efficient watershed delineation using ArcView and spatial analyst. In: *Proceedings of the 17th Annual ESRI User, User Conference*, San Diego, CA.

El Alfy, M. 1998 Applications of engineering geology on the geomorphological and hydrogeological situations of the area between Rafah and Ras El- Naqab. MSc Thesis, Faculty of Science, Mansoura University, Egypt, 301 p.

El Bastawesy, M., White, K. & Nasr, A. 2009 Integration of remote sensing and GIS for modelling flash floods in Wadi Hudain catchment, Egypt. *Hydrol. Process.* **23**, 1359–1368.

El Bastawesy, M., Al Harbi, K. & Habeebullah, T. 2012 The hydrology of Wadi Ibrahim Catchment in Makkah City, the Kingdom of Saudi Arabia: the interplay of urban development and flash flood hazards. *Life Sci. J.* **9** (1), 580–589.

ERDAS 2010 ERDAS Field Guide. Manager, Technical Documentation. ERDAS, Inc., 811 p.

ESRI Inc. 2012 *Arcgis 10.0 manual user's guide, 3D Analyst Tutorial*. Esri, Redlands, CA, USA, 196 p.

Evans, D., Lathon, R., Senalp, M. & Conally, T. 1991 *Stratigraphy of the Wajid Sandstone of South-western Saudi Arabia*. Paper Society of Petroleum Engineers, Middle East Oil Show, Bahrain, SPE 21449, pp. 947–960.

Foody, G., Ghoneim, E. & Arnell, N. 2004 Predicting locations sensitive to flash flooding in an arid environment. *J. Hydrol.* **292** (1–4), 48–58.

Gheith, H. & Sultan, M. 2002 Construction of a hydrologic model for estimating Wadi runoff and groundwater recharge in the Eastern Desert, Egypt. *J. Hydrol.* **263**, 36–55.

Graf, L. 1988 *Fluvial Processes in Dryland Rivers*. Springer-Verlag, New York, 387 p.

Herschy, R. 2002 The world's maximum observed floods. In: *The Extremes of the Extremes: Extraordinary Floods* (A. Snorrason, H. P. Finnsdottir & M. Moss, eds), IAHS Publication 271, Wallingford, UK, pp. 355–360.

Hublart, P., Ruelland, D., Garc'la De Cortázar Atauri, I. & Ibacach, A. 2015 Reliability of a conceptual hydrological model in a semi-arid Andean catchment facing water-use changes. *Proc. IAHS* **371**, 203–209.

Jarrett, R. 1990 Hydrologic and hydraulic research in mountain rivers. *Water Resour. Bull.* **26** (3), 419–429.

Kibler, D., Froelich, C. & Aron, G. 2007 Analyzing urbanization impacts on Pennsylvania flood peaks. *J. Am. Water Resour. Assoc.* **17** (2), 270–274.

Liu, Y. & Sun, F. 2010 Sensitivity analysis and automatic calibration of a rainfall-runoff model using multi-objectives. *Ecol. Inf.* **5**, 304–310.

Liu, Y., De Smedt, F., Hoffmann, F. & Pfister, L. 2004 Assessing land-use impacts on flood processes in complex terrain by using GIS and modeling approach. *Environ. Model. Assess.* **9**, 227–235.

Mark, D. 1984 Automated detection of drainage networks from digital elevation models. *Cartographica* **2**, 168–178.

Michaud, J. & Sorooshian, S. 1994 Comparison of simple versus complex distributed runoff models on a midsized semiarid watershed. *Water Resour. Res.* **30** (3), 593–605.

Milzow, C., Kgotlhang, L., Kinzelbach, W., Meier, P. & Bauer-Gottwein, P. 2009 The role of remote sensing in hydrological modelling of the Okavango Delta, Botswana. *J. Environ. Manage.* **90**, 2252–2260.

Mishra, S. & Singh, V. 2004 Longterm hydrological simulation based on the Soil Conservation Service curve number. *Hydrol. Process.* **18**, 1291–1313.

Nirupama, N. & Simonovic, S. 2007 Increase of flood risk due to urbanization: a Canadian example. *Nat. Hazards* **40**, 25–41.

Oba, G. 2001 The effect of multiple droughts on cattle in Obbu, Northern Kenya. *J. Arid Environ.* **49**, 375–386.

Ozturk, M., Copty, N. & Saysel, A. 2013 Modeling the impact of land use change on the hydrology of a rural watershed. *J. Hydrol.* **497**, 97–109.

PME 2011 *Metrological data of SA-101 Station, Jazan Area*. Presidency of Meteorology and Environment, Riyadh, KSA.

Reich, B. 1963 Short-duration rainfall intensity estimation and other design aids for regions of spare data. *J. Hydrol.* **1**, 3–28.

Rodier, J. 1985 Aspects of arid zone hydrology. In: *Facets of Hydrology*, Vol. II (J. C. Rodda, ed.), Wiley, Chichester, pp. 205–247.

Saghafian, B., Farazjoo, H., Bozorgy, B. & Yazdandoost, F. 2008 Flood intensification due to changes in land use. *Water Resour. Manage.* **22**, 1051–1067.

Scharffenberg, W. 2013 *Hydrologic modeling system HEC-HMS v4.0 user's manual*. USACE-HEC, Davis, CA, USA, 426 p.

Scipal, K., Scheffler, C. & Wagner, W. 2005 Soil moisture-runoff relation at the catchment scale as observed with coarse

resolution microwave remote sensing. *Hydrol. Earth Syst. Sci.* **9**, 173–183.

SCS 1972 *National Engineering Handbook*, Section 4, Hydrology, US Department of Agriculture, US Government Printing Office, Washington, DC.

Shang, J. & Wilson, J. 2009 Watershed urbanization and changing flood behavior across the Los Angeles metropolitan region. *Nat. Hazards* **48**, 41–57.

Sorman, A. & Abdulrazzaq, J. 1993 Infiltration-recharge through wadi beds in arid region. *Hydrol. Sci. J.* **38** (3), 173–186.

Tooth, S. 2000 Process, form, and change in dry land rivers: a review of recent research. *Earth Sci. Rev.* **51**, 67–107.

USACE (US Army Corps of Engineers) 2010 *HEC-HMS, User's Manual Version 3.5, 2010*. Hydrologic Engineering Center, Davis, CA, USA.

USDA 1986 Urban Hydrology for Small Watersheds, US Department of Agriculture, Natural Resources Conservation Services, Conservation Engineering Division, Technical Release TR-55, 164 p.

Wagener, T., Wheater, H. & Gupta, H. 2004 *Rainfall-Runoff Modelling in Gauged and Ungauged Catchments*. Imperial College Press, London, 330 p.

Walters, O. 1990 Transmission losses in arid region. *Hydraul. Engng.* **116** (1), 127–138.

Wheater, S. & Bell, N. 1983 Northern Oman flood study. *Proc. Inst. Civil Engrs* **2** (75), 453–473.

Wise, S. 2000 Assessing the quality for hydrological applications of digital elevation models derived from contours. *Hydrol. Process.* **14**, 1909–1929.

WMS-8.3 2010 Watershed Modeling System, Tutorials. Aquaveo, LLC, Provo, UT. Vol. 2, 121 p.

First received 24 June 2015; accepted in revised form 29 November 2015. Available online 29 January 2016